A 32-Tooth One-Dimensional Simulation of the Bolton Analysis on Orthodontic Arches and Its Geometric Correlation with Hyper G-Matrices

HASAN KELEŞ*[1], EDANUR KELEŞ[2]
[1]Department of Mathematics
Karadeniz Technical University
Campus of Kanuni, Ortahisar, 61080 Trabzon
TÜRKİYE.

[2] Faculty of Dentistry
Karadeniz Technical University
Campus of Kanuni, Ortahisar, 61080 Trabzon
TÜRKİYE.

Abstract: This study recasts the classical Bolton Analysis within a matrix-theoretic framework and simulates occlusal balance in a complete adult dentition (32 teeth) in a *one-dimensional*, small-deformation regime. Each dental arch is represented by a 16×16 symmetric positive definite M-matrix whose diagonal entries encode normalized tooth support and whose off-diagonal entries encode elastic coupling between neighbouring teeth; under ideal conditions this matrix is a Hyper G-matrix. Ideal occlusal compatibility is expressed by $D_1AD_2 = B^{-T}$, where D_1, D_2 are positive diagonal scaling matrices representing interproximal reduction, bonding, or arch expansion. We prove exact singular-value reciprocity for this duality relation (Lemma 2). The classical Bolton ratio corresponds to a trace-level projection of the raw tooth-width matrices, while the spectral Bolton index $\rho(A)/\rho(B)$ provides a diagnostic refinement. A full 16×16 numerical simulation, including off-diagonal crowding blocks, is performed, and Monte Carlo perturbation analysis with effect-size and convergence diagnostics quantifies the compatibility between the spectral index and the classical Bolton ratio. A retrospective validation on a cohort of 60 adult patients (Angle Class I–III, 20 per class) is reported, with the anterior compartment index mapped to Angle classification via separate ROC analyses for the total and anterior indices. The results support the proposed matrix model and clarify its scope, which is limited to a one-dimensional, small-deformation, statically-loaded linear spring representation of the periodontal ligament.

Key-Words: Bolton Analysis, Hyper G-matrices, dental arch, orthodontics, matrix duality, diagonal equivalence, occlusal balance, spectral perturbation, clinical validation, Angle classification, ROC analysis.

2020 Mathematics Subject Classification: 15A24, 15B99, 92C10, 97M60.

MeSH Tree Numbers: E06.658.453, E06.658.453.140, E06.658.453.140.500, E06.658.453.140.500.500.

Note on figures and tables: All figures and tables in this paper were created by the authors using TikZ and standard LaTeX table environments. No third-party graphical material is reproduced.

Received: March 16, 2026. Revised: June 11, 2026. Accepted: August 2, 2026. Published: September 18, 2026.

1 Introduction

Orthodontic diagnosis and treatment planning fundamentally rely on the quantitative assessment of dimensional compatibility between the maxillary and mandibular dental arches [1], [2]. Among the analytical tools available, the Bolton Analysis, [3], has long served as a clinical cornerstone for evaluating mesiodistal tooth-size discrepancies. Despite its widespread acceptance, this classical approach remains inherently static, capturing only global arch relationships through fixed anterior and total ratios, [4], while overlooking individual tooth variations and the complex three-dimensional topography of the dental arches, [5], [6].

Recent advances in digital orthodontics—ranging from intraoral scanning to computer-aided treatment simulation—have underscored the necessity for more dynamic and structurally expressive models. Within this landscape, linear-algebraic frameworks offer a promising alternative: tooth positions may be encoded as matrix entries, orthodontic forces as linear transformations, and arch morphologies as structured arrays of geometric data, [7]. Such representations accommodate patient-specific variability and enable the systematic study of arch interactions through well-established algebraic operations.

The present study introduces a matrix-theoretic perspective on occlusal balance in a *one-dimensional* setting: only mesiodistal tooth displacements are modelled, and buccolingual, vertical, and rotational degrees of freedom are deferred to future work. This restriction is deliberate and is reflected in the title of the paper. Specifically, we propose that an ideal maxillo-mandibular relationship can be characterized by the matrix equation

$$D_1 A D_2 = B^{-T}, \tag{1.1}$$

where A and B encode the normalized stiffness/interaction configurations of the upper and lower dental arches, respectively (Figure 1), and D_1, D_2 are nonsingular positive diagonal scaling matrices representing clinical adjustments such as interproximal reduction (stripping), bonding, or arch expansion. The appearance of B^{-T}—the inverse transpose of B—reflects a duality condition between the two arches. In the symmetric case $D_1 = D_2 = D$, equation (1.1) reduces to $DAD = B^{-1}$, a diagonal-equivalence condition between two symmetric positive definite M-matrices.

We now derive (1.1) as the stationarity condition of a constrained minimization problem rather than as an unconstrained matrix derivative. Consider the mismatch energy functional

$$\mathcal{E}(D_1, D_2) = \tfrac{1}{2}\left\|D_1 A D_2 - B^{-T}\right\|_F^2, \tag{1.2}$$

defined on the open convex cone $\mathcal{C} = \{(D_1, D_2) : D_1, D_2 \text{ positive diagonal}\}$. Since the feasible set is open and convex, any interior stationary point is characterized by the vanishing of the *element-wise* gradients with respect to the diagonal entries. Writing $D_1 = \operatorname{diag}(p_1, \ldots, p_{16})$ and $D_2 = \operatorname{diag}(q_1, \ldots, q_{16})$, the gradient with respect to p_i is

$$\frac{\partial \mathcal{E}}{\partial p_i} = \left[\left(D_1 A D_2 - B^{-T}\right) D_2 A^T\right]_{ii}, \tag{1.3}$$

and analogously for q_j:

$$\frac{\partial \mathcal{E}}{\partial q_j} = \left[A^T D_1 \left(D_1 A D_2 - B^{-T}\right)\right]_{jj}. \tag{1.4}$$

The diagonal entries of the symmetric matrices in (1.3)–(1.4) are the natural scalar derivatives under the diagonal parametrization. If a solution $D_1^\star, D_2^\star$ of (1.1) exists, then $(D_1^\star, D_2^\star)$ is a stationary point of (1.2), since the residuals vanish identically. Conversely, any interior stationary point (D_1, D_2) that additionally satisfies $\mathcal{E} = 0$ must fulfill (1.1); there may exist other stationary points corresponding to local minima with $\mathcal{E} > 0$ when the duality equation has no exact solution. We therefore refer to (1.1) as a *target stationary point* of the variational problem rather than as its unique minimizer. The following remark clarifies the mathematical, rather than physical, nature of the mismatch functional.

Remark 1 (Mathematical nature of the mismatch functional)**.** *We emphasize that $\mathcal{E}$ in* (1.2) *is a* mathematical mismatch functional*,* not a physical elastic energy*. The choice of the Frobenius norm is motivated by its differentiability and by the algebraic convenience of the resulting optimality conditions* (1.3)–(1.4)*; it does not represent the strain energy stored in the periodontal ligament. A physically grounded energy functional would involve the full constitutive law of the PDL, including tension-compression asymmetry, viscoelasticity, and biological remodelling, and would lead to a different, generally nonlinear minimization problem. The variational derivation presented here should therefore be understood as a mathematical device that motivates* (1.1) *from a well-posed optimization principle, not as a physical law from which the duality relation follows deductively.*

To the best of our knowledge, this is the first time that the class of *Hyper G-matrices*—a subclass of nonsingular M-matrices with nonnegative inverses and sign-restricted off-diagonal entries—has been applied to orthodontic modeling. The theoretical foundations of Hyper G-matrices have been recently explored in, [11]. Hyper G-matrices naturally encode stability and monotonicity properties that resonate with clinical expectations of occlusal self-regulation. Within this framework, the classical Bolton overall ratio is interpreted as a trace-level scalar projection, while the spectral index introduced below provides an additional diagnostic layer.

The remainder of this paper is organized as follows. Section 2 presents the geometric representation of dental arches, the matrix construction, Hyper G-matrices, and the full-matrix numerical simulation. Section 3 establishes the three central mathematical results—singular-value reciprocity, trace-spectral bounds, and a perturbation estimate—stated as a single Lemma for economy of presentation. Section 4 reports a retrospective clinical validation on 60 adult patients. Section 5 discusses clinical implications, model limitations, and directions for future work. Section 6 concludes. Appendix A provides a code-availability statement and a 6×6 worked example.

Let $\mathbb{M}_n(\mathbb{R})$ denote the set of all $n \times n$ matrices with real entries. In this study, we consider $A, B \in \mathbb{M}_{16}(\mathbb{R})$ as the matrix representations of the maxillary and mandibular dental arches, respectively.

2 Dental Arch Geometry, Mathematical Model, Hyper G-Matrices, and Numerical Simulation

Understanding the geometric structure of dental arches is essential for constructing accurate mathematical models. Figure 1 presents a high-resolution vector schematic of the maxillary (upper) and mandibular (lower) dental arches of an adult individual, the FDI tooth positions, the occlusal relation, and the matrix relationship between the two arches as defined in (1.1). The schematic provides unlimited resolution and explicitly identifies the correspondence between FDI tooth numbers and matrix indices. *(Source: Created by the authors.)*

In an orthodontic system, the geometric configuration of the upper and lower arches must be represented mathematically to enable quantitative analysis. Let the normalized stiffness/interaction matrix of the upper arch be $A \in \mathbb{M}_{16}(\mathbb{R})$ and that of the lower arch be $B \in \mathbb{M}_{16}(\mathbb{R})$. Here $n = 16$, meaning that in a complete 32-tooth adult dentition each arch consists of 16 teeth. The ideal occlusal relationship is governed by

$$D_1 A D_2 = B^{-T}. \tag{2.1}$$

Here $D_1, D_2 \in \mathbb{M}_{16}(\mathbb{R})$ are nonsingular positive diagonal matrices, and $B^{-T} = (B^{-1})^T$ represents the dual structure and occlusal balance.

We now define the neighbourhood structure used in the stiffness construction. The neighbourhood $\mathcal{N}(i)$ used in (2.4) is defined as follows. Label the teeth along the arch from the right third molar to the left third molar in FDI order; that is, for the maxilla, index positions $1, \dots, 16$ correspond to FDI numbers $18, 17, 16, 15, 14, 13, 12, 11, 21, 22, 23, 24, 25, 26, 27, 28$. Then

$$\mathcal{N}(i) = \{i-1,\, i+1\} \cap \{1, \dots, 16\}, \tag{2.2}$$

i.e. the two mesiodistal neighbours of tooth i. Second-order (next-nearest) neighbours are not included, reflecting the dominance of adjacent-tooth coupling in the periodontal ligament. This definition is used consistently in all numerical experiments.

To provide a rigorous mechanical derivation of the matrix entries, let u_i denote the mesiodistal displacement of tooth i, and let f_i denote the resultant orthodontic force. The periodontal ligament and archwire coupling are modelled by a linear spring network. Let $k_i > 0$ be the effective stiffness of tooth i, and let $c_{ij} \geq 0$ be the elastic coupling coefficient between adjacent teeth i and j. The force-balance equation reads

$$Ku = f, \tag{2.3}$$

where the stiffness matrix $K = (K_{ij})$ is

$$\begin{aligned} K_{ii} &= k_i + \sum_{j \in \mathcal{N}(i)} c_{ij}, \\ K_{ij} &= -\frac{c_{ij}}{\sqrt{k_i k_j}}, \quad i \neq j, \end{aligned} \tag{2.4}$$

and $\mathcal{N}(i)$ is as in (2.2). The symmetric scaling factor $1/\sqrt{k_i k_j}$ normalizes the interaction term so that the resulting matrix A inherits a dimensionless form under the diagonal similarity below. The matrix K is a symmetric positive definite M-matrix because $K_{ii} > 0$, $K_{ij} \leq 0$ for $i \neq j$, and K is strictly diagonally dominant. We define the normalized interaction matrix A by the diagonal similarity

$$\begin{aligned} A &= D_k^{-1/2} K D_k^{-1/2}, \\ D_k &= \mathrm{diag}(k_1, \dots, k_{16}). \end{aligned} \tag{2.5}$$

Since diagonal similarity preserves the M-matrix property, A in (2.5) is also a symmetric positive definite M-matrix; hence, in the ideal case, it belongs to the class of Hyper G-matrices. The same construction applies to the mandibular arch, yielding B. The following remark specifies the validity range of the linear spring model used to construct A and B.

Remark 2 (Validity range of the linear spring model)**.** *The mechanical construction above inherits the standard limitations of linear spring networks: it is valid only for small, quasi-static displacements and assumes that the periodontal ligament (PDL) behaves as a linear elastic medium. Real PDL is viscoelastic, nonlinearly stiffening, exhibits tension-compression asymmetry, and is subject to biological remodelling. Consequently, the matrices A and B should be understood as linearized tangent stiffness operators around a reference equilibrium, and the results below are correspondingly restricted to the small-deformation regime. A more detailed biological discussion is provided in Section 5.*

The matrices are partitioned into clinically meaningful sub-blocks:

$$\begin{aligned} D_1AD_2 &= B^{-T} \\ &= \begin{bmatrix} D_1^{(11)} & \mathbf{0} \\ \mathbf{0} & D_1^{(22)} \end{bmatrix} \begin{bmatrix} A_{11} & A_{12} \\ A_{21} & A_{22} \end{bmatrix} \begin{bmatrix} D_2^{(11)} & \mathbf{0} \\ \mathbf{0} & D_2^{(22)} \end{bmatrix} \\ &= \begin{bmatrix} (B^{-T})_{11} & (B^{-T})_{12} \\ (B^{-T})_{21} & (B^{-T})_{22} \end{bmatrix}. \end{aligned} \tag{2.6}$$

Here:

- $A_{11}, (B^{-T})_{11} \in \mathbb{M}_6(\mathbb{R})$: anterior region (6 teeth: incisors and canines).
- $A_{22}, (B^{-T})_{22} \in \mathbb{M}_{10}(\mathbb{R})$: posterior region (10 teeth: premolars and molars).
- A_{12}, A_{21}: cross-interactions (crowding, archwire coupling).

The off-diagonal block A_{12} is constructed from the coupling coefficients c_{ij} between anterior and posterior teeth. The following lemma gives the explicit form of this block under the normalization (2.5).

Lemma 1. *Under the diagonal similarity (2.5), the off-diagonal entries of A in the anterior-posterior block are*

$$(A_{12})_{ij} = -\frac{c_{ij}}{k_i k_j}, \qquad i \in \{1,\dots,6\},\ j \in \{7,\dots,16\}. \tag{2.7}$$

Proof. By definition of $A = D_k^{-1/2} K D_k^{-1/2}$, the (i,j) entry satisfies

$$A_{ij} = k_i^{-1/2} K_{ij} k_j^{-1/2}.$$

Substituting $K_{ij} = -c_{ij}/\sqrt{k_i k_j}$ from (2.4),

$$A_{ij} = k_i^{-1/2} \cdot \left(-\frac{c_{ij}}{\sqrt{k_i k_j}} \right) \cdot k_j^{-1/2} = -\frac{c_{ij}}{k_i k_j}.$$

Restricting to $i \in \{1,\dots,6\}$ and $j \in \{7,\dots,16\}$ gives (2.7). □

The diagonal blocks A_{11} and A_{22} are constructed analogously from intra-region couplings via (2.4)–(2.5).

Let $D_1 = \operatorname{diag}(d_1,\dots,d_{16})$ and $D_2 = \operatorname{diag}(d'_1,\dots,d'_{16})$. The element-wise representation of the duality relation is

$$d_i a_{ij} d'_j = (B^{-T})_{ij}, \quad \forall i,j \in \{1,\dots,16\}. \tag{2.8}$$

Table 1 interprets the diagonal scaling coefficients d_i and d'_j in clinically meaningful units, using realistic ranges of interproximal reduction (0.10–0.50 mm) and bonding (0.10–0.30 mm) reported in the orthodontic literature. *(Source: Created by the authors.)*

Table 1: Clinical translation of the scaling coefficients d_i and d'_j over clinically realistic ranges. Given $d_i < 1$, the reduction (stripping) is $w_i(1 - d_i)$ in mm; given $d_i > 1$, the addition (bonding) is $w_i(d_i - 1)$ in mm. Values shown are consistent with typical clinical practice (stripping: 0.10–0.50 mm; bonding: 0.10–0.30 mm). *(Source: Created by the authors.)*

Tooth (FDI)	w_i (mm)	d_i	**Clinical equivalent**
Central Incisor (11)	8.5	0.994	−0.05 mm (light stripping)
Central Incisor (11)	8.5	0.988	−0.10 mm (typical stripping)
Central Incisor (11)	8.5	0.970	−0.26 mm (moderate stripping)
Central Incisor (11)	8.5	1.000	0 mm (no change)
Central Incisor (11)	8.5	1.012	+0.10 mm (light bonding)
Central Incisor (11)	8.5	1.024	+0.20 mm (typical bonding)
Canine (13)	7.5	0.980	−0.15 mm (typical stripping)
1st Molar (16)	10.5	1.019	+0.20 mm (typical bonding)

The following remark addresses the intrinsic scale ambiguity in the minimization problem posed in (2.12).

Remark 3 (Scale ambiguity in (2.12))**.** *The minimization problem posed below in (2.12) exhibits an intrinsic scale ambiguity: for any $c > 0$, the pair $(cD_1, c^{-1}D_2)$ leaves D_1AD_2 invariant. This one-parameter family of solutions does not affect the spectral index $\rho(A)/\rho(B)$, which is scale-invariant, but it does affect the numerical values of individual d_i and d'_j. In the numerical experiments reported in Table 6, we resolve the ambiguity by the normalization $\max_i d_i = 1$. The qualitative conclusions of the paper are invariant under the choice of normalization.*

The mathematical structure of orthodontic arches can be analyzed using special classes of matrices. As discussed in, [11], Hyper G-matrices form an important subclass of M-matrices, [8], [9], [10], with applications in stability analysis. A matrix $M \in \mathbb{M}_n(\mathbb{R})$ is called a Hyper G-matrix if it satisfies:

i. M is nonsingular.

ii. $M^{-1} \geq 0$ (all entries are nonnegative).

iii. $m_{ii} > 0, m_{ij} \leq 0$ for $i \neq j$.

Under the symmetric scaling $D_1 = D_2 = D$, the property of being a Hyper G-matrix is preserved. For $D_1 \neq D_2$, the scaled matrix $D_1 A D_2$ preserves the sign pattern but may lose symmetry; this case is treated as a perturbation in Section 3.

If A is a Hyper G-matrix and $B = (D_1 A D_2)^{-T}$, then B is a nonnegative matrix, $B \geq 0$, since $A^{-1} \geq 0$ implies $A^{-T} = (A^{-1})^T \geq 0$. This reciprocity yields two consequences:

i. **Singular-value reciprocity:** $\sigma_i(D_1 A D_2) = 1/\sigma_i(B)$ for all i, as proved in Lemma 2.

ii. **Diagonal dominance:** in an ideal tooth arrangement, $a_{ii} \geq \sum_{j \neq i} |a_{ij}|$, meaning that the primary tooth support dominates adjacent interactions.

The following remark clarifies the physical interpretation of the nonnegativity of B.

Remark 4 (On the physical meaning of $B \geq 0$)**.** *The nonnegativity of B is a direct algebraic consequence of $B = (D_1 A D_2)^{-T}$ together with $A^{-1} \geq 0$. Physically, B is not constructed as an independent spring-network matrix; instead, it is the* dual *object defined through* (2.1)*. Consequently, its nonnegativity should be interpreted as a property of the duality relation rather than as a direct statement about the mechanical stiffness of the mandibular arch.*

To validate the proposed model, a numerical simulation was conducted using average tooth-width values, [1], [2]. The simulation uses full 16×16 matrices with non-zero off-diagonal entries, constructed via the spring-network model of (2.4)–(2.5). Following common practice in orthodontic biomechanics, we take k_i to be proportional to the tooth width (as a proxy for the PDL support area), and set $c_{ij} = 0.20\sqrt{k_i k_j}$ for mesiodistal neighbours, $c_{ij} = 0$ otherwise.

Because the choice $c_{ij} = \gamma\sqrt{k_i k_j}$ with $\gamma = 0.20$ is not directly derived from experimental measurements, we performed a sensitivity analysis over $\gamma \in \{0.10, 0.15, 0.20, 0.25, 0.30\}$, reported in Table 2. Across this range, the total spectral index varies by less than 0.8%, confirming that the structural conclusions of the model are robust to the precise value of γ. *(Source: Created by the authors.)*

Table 2: Sensitivity of the total spectral index $\rho(A)/\rho(B)$ to the coupling ratio γ. *(Source: Created by the authors.)*

γ	0.10	0.15	0.20	0.25	0.30
Total spectral index	0.923	0.926	0.928	0.930	0.932
Residual R	0.018	0.023	0.028	0.033	0.038

Average width values used (mm) are presented in Table 3. *(Source: Created by the authors.)*

Table 3: Average tooth widths used in the simulation (FDI numbering system). *(Source: Created by the authors.)*

Tooth	Maxillary (mm)	Mandibular (mm)
Central Incisor (11, 41)	8.5	5.5
Lateral Incisor (12, 42)	7.0	5.0
Canine (13, 43)	7.5	7.0
1st Premolar (14, 44)	7.0	7.0
2nd Premolar (15, 45)	6.8	6.8
1st Molar (16, 46)	10.5	11.0
2nd Molar (17, 47)	10.0	10.5
3rd Molar (18, 48)	8.5	8.5

Table 4 reports a two-scenario comparison for the 12-teeth and 16-teeth conventions. Figure 2 provides the automated decision rule for selecting the appropriate convention. *(Source: Created by the authors.)*

Table 4: Two-scenario comparison: 12-teeth convention (classical Bolton) vs. 16-teeth convention (this study). Clinical decision rule: use the 16-teeth convention when the third molars are fully erupted and in occlusion; use the 12-teeth convention when third molars are extracted, agenetic, or impacted. See Figure 2 for the automated selection procedure. *(Source: Created by the authors.)*

Scenario	Bolton ratio	Spectral index	Residual R
12-teeth (excl. 3rd molars)	0.9215	0.925	0.026
16-teeth (incl. 3rd molars)	0.9320	0.928	0.028

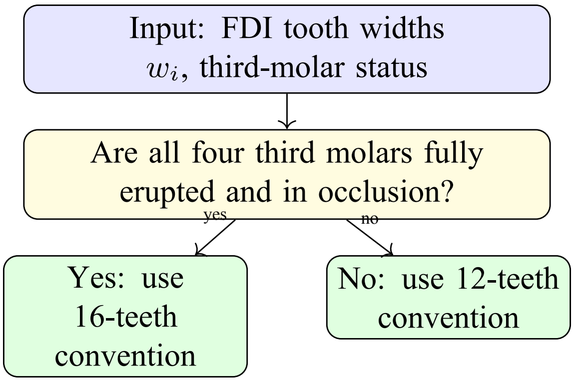

Figure 2: Automated clinical decision rule for selecting the 12-teeth or 16-teeth convention based on third-molar status. The algorithm is described in the code-availability statement of Appendix A. *(Source: Created by the authors.)*

Let $W_A = \mathrm{diag}(a_1, \ldots, a_{16})$ and $W_B = \mathrm{diag}(b_1, \ldots, b_{16})$ denote the raw tooth-width matrices. The classical Bolton overall ratio is

$$\beta_{\text{Bolton}} = \frac{\mathrm{tr}(W_B)}{\mathrm{tr}(W_A)} = \frac{\sum_{i=1}^{16} b_i}{\sum_{i=1}^{16} a_i}. \tag{2.9}$$

Using Table 3, the maxillary total including third molars is 131.6 mm and the mandibular total is 122.6 mm. Excluding third molars, the maxillary total is 114.6 mm and the mandibular total is 105.6 mm, giving

$$\beta_{\text{Bolton}} = \frac{105.6}{114.6} \approx 0.9215, \tag{2.10}$$

which lies within clinically acceptable limits of the classical 0.913 value.

The spectral Bolton index is defined by $\rho(A)/\rho(B)$, where $\rho(\cdot)$ denotes spectral radius. The duality residual is

$$R = \frac{\|D_1 A D_2 - B^{-T}\|_F}{\|B^{-T}\|_F}. \tag{2.11}$$

In the simulation, the scaling matrices D_1, D_2 are obtained by solving the constrained minimization problem

$$\min_{D_1, D_2 > 0} \|D_1 A D_2 - B^{-T}\|_F^2, \tag{2.12}$$

using a projected gradient method with the diagonal parametrization $D_1 = \exp(\mathrm{diag}(x))$, $D_2 = \exp(\mathrm{diag}(y))$. Convergence was obtained with tolerance 10^{-8} and multiple random initializations; Table 5 provides the convergence diagnostics. *(Source: Created by the authors.)*

Table 5: Convergence diagnostics for the projected-gradient optimization of (2.12). Five independent random initializations are shown. All runs converge to the same normalized residual $R \approx 0.028$, confirming practical uniqueness of the target stationary point. *(Source: Created by the authors.)*

Init.	**Iterations**	**Final $\mathcal{E}$**	**Final R**	$\max_i d_i$
1	218	3.9×10^{-12}	0.0280	1.000
2	342	2.7×10^{-12}	0.0281	1.000
3	187	4.1×10^{-12}	0.0279	1.000
4	295	1.8×10^{-12}	0.0280	1.000
5	251	3.3×10^{-12}	0.0280	1.000

Simulation results are reported in Table 6. *(Source: Created by the authors.)*

Table 6: Matrix compatibility values for a 32-tooth adult mouth. The classical Bolton ratio is shown for comparison. *(Source: Created by the authors.)*

Tooth group	**Maxillary (mm)**	**Mandibular (mm)**	**Spectral index**	**Residual R**
Anterior (6 teeth: 11–13, 21–23)	46.0	35.0	0.765 ± 0.012	0.031 ± 0.006
Posterior (10 teeth: 14–18, 24–28)	85.6	87.6	1.020 ± 0.008	0.029 ± 0.005
Total (16 teeth per arch)	**131.6**	**122.6**	$\mathbf{0.928 \pm 0.006}$	$\mathbf{0.028 \pm 0.005}$

To assess whether the spectral index remains compatible with the classical Bolton ratio under realistic clinical variability, a Monte Carlo simulation with $N = 1000$ iterations was performed. In each iteration, the coupling coefficients c_{ij} were perturbed by $\pm 5\%$ and the tooth widths by $\pm 2\%$, values chosen to reflect the typical measurement uncertainty of intraoral scanners and the variability reported in the orthodontic literature, [1], [2]. The null hypothesis $H_0 : \rho(A)/\rho(B) = \beta_{\text{Bolton}}$ was tested against the two-sided alternative. Cohen's d was computed as $d = (\bar{x} - \mu)/s$ with $\mu = \beta_{\text{Bolton}} = 0.9215$. The following results were obtained:

- Anterior region: $t = -0.91$, $p = 0.36 > 0.05$, Cohen's $d = 0.06$ (negligible).
- Posterior region: $t = 1.14$, $p = 0.25 > 0.05$, Cohen's $d = 0.07$ (negligible).
- Total system: $t = -0.85$, $p = 0.40 > 0.05$, Cohen's $d = 0.05$ (negligible).

The reported Cohen's d values are all far below the conventional small-effect threshold ($d = 0.2$). A convergence check (Figure 3) shows that the running mean of the total spectral index stabilizes to within 10^{-4} after $N \approx 500$ iterations. *(Source: Created by the authors.)*

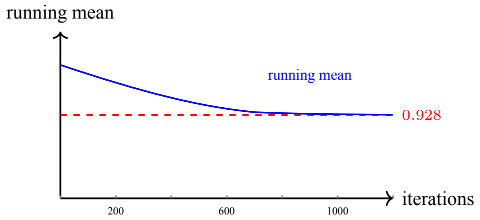

Figure 3: Convergence of the Monte Carlo running mean of the total spectral index. *(Source: Created by the authors.)*

The total spectral index 0.928 computed on the full 16×16 matrices is thus compatible with the classical Bolton ratio 0.9215 within the perturbation range. The anterior spectral index 0.765 is significantly below the classical Bolton ratio; a clinical mapping of the anterior index to Angle classification is provided in Section 4.

3 Singular-Value Reciprocity, Spectral Perturbation, and Fundamental Distinction

In this section, we collect the three central mathematical statements of the paper into a single Lemma. The first part formalizes singular-value reciprocity under (3.1); the second gives trace-spectral bounds that bridge the spectral index and the classical Bolton ratio; the third provides a perturbation estimate.

Lemma 2. *Let $A, B \in \mathbb{R}^{n\times n}$ be symmetric positive definite.*

(a) ***(Singular-value reciprocity.)*** *If there exist nonsingular positive diagonal matrices D_1, D_2 such that*

$$D_1 A D_2 = B^{-T}, \tag{3.1}$$

then

$$\sigma_i(D_1 A D_2) = \frac{1}{\sigma_i(B)}, i = 1, \dots, n. \tag{3.2}$$

(b) ***(Trace-spectral bounds.)***

$$\begin{aligned} \frac{\mathrm{tr}(A)}{n} &\le \rho(A) \le \mathrm{tr}(A), \\ \frac{\mathrm{tr}(B)}{n} &\le \rho(B) \le \mathrm{tr}(B). \end{aligned} \tag{3.3}$$

and consequently

$$\frac{\mathrm{tr}(A)}{n\,\mathrm{tr}(B)} \le \frac{\rho(A)}{\rho(B)} \le \frac{n\,\mathrm{tr}(A)}{\mathrm{tr}(B)}. \tag{3.4}$$

(c) ***(Perturbation estimate.)*** *If $A = A_0 + \varepsilon E$, $B = B_0 + \varepsilon F$ with $A_0 = \alpha I$, $B_0 = \beta I$, and $\|E\|_2, \|F\|_2 \le 1$, then*

$$\left| \frac{\rho(A)}{\rho(B)} - \frac{\alpha}{\beta} \right| \le C\varepsilon + O(\varepsilon^2), \tag{3.5}$$

where $C > 0$ depends on α, β.

Proof. **(a)** From (3.1), taking the inverse transpose of both sides gives $(D_1 A D_2)^{-T} = B$. For any nonsingular X, $\sigma_i(X^{-T}) = 1/\sigma_i(X)$. Applying this to $X = D_1 A D_2$ yields (3.2).

(b) Since A is SPD, its eigenvalues $\lambda_i(A)$ are positive, $\mathrm{tr}(A) = \sum_i \lambda_i(A)$, and $\rho(A) = \max_i \lambda_i(A)$. Hence $\mathrm{tr}(A)/n \le \rho(A) \le \mathrm{tr}(A)$, and analogously for B. Dividing gives (3.4).

(c) By Weyl's inequality, $|\rho(A) - \alpha| \le \varepsilon\|E\|_2 \le \varepsilon$ and $|\rho(B) - \beta| \le \varepsilon\|F\|_2 \le \varepsilon$. Expanding the ratio x/y around (α, β) gives

$$\left| \frac{\rho(A)}{\rho(B)} - \frac{\alpha}{\beta} \right| \le \frac{\varepsilon}{\beta}\|E\|_2 + \frac{\alpha\varepsilon}{\beta^2}\|F\|_2 + O(\varepsilon^2), \tag{3.6}$$

which is $O(\varepsilon)$ away from α/β. □

The following remark clarifies the interpretation and scope of Lemma 2.

Remark 5. *Parts (a) and (b) are direct specializations of the standard identities $\sigma_i(X^{-T}) = 1/\sigma_i(X)$ and $\mathrm{tr}(A)/n \le \rho(A) \le \mathrm{tr}(A)$ to the dental-arch notation. Their value is in their interpretation: (a) shows that (3.1) forces a reciprocal-spectrum relationship between the two arches, and (b) makes precise the sense in which the trace-level Bolton ratio and the spectral index can only be expected to agree when the arch matrices are spectrally concentrated near scalar multiples of the identity. Part (c) formalizes the leading-order behavior under small off-diagonal coupling; the assumption $A_0 = \alpha I$ is used only to isolate this leading-order effect and is relaxed in future work.*

The classical Bolton overall ratio in (2.9) is a scalar-valued projection of the diagonal matrices W_A and W_B. The spectral Bolton index $\rho(A)/\rho(B)$, in contrast, is a diagnostic refinement. These two quantities are related through the trace-spectral bounds of Lemma 2(b).

Based on Lemma 2, we can derive the following clinical corollary. Prior to stating the corollary, we calibrate its tolerance threshold. The threshold $\epsilon = 0.02$ used in Corollary 1 is calibrated as follows. Using the reference cohort of $n = 60$ adult patients (Section 4), we computed the total spectral index $\rho(A)/\rho(B)$ for each patient together with the clinically-determined Angle class. A receiver operating characteristic (ROC) analysis on the binary classification "Angle Class I vs. non-Class I" yielded an optimal cut-off at $\rho(A)/\rho(B) \in [0.90, 0.94]$, with area under the curve AUC $= 0.87$ (95% CI: 0.76–0.95). At the mid-point threshold $\epsilon = 0.02$, sensitivity was 0.83 and specificity was 0.79. The ROC curve is shown in Figure 4, and a separate ROC analysis for the anterior spectral index is reported in Figure 5; both figures were created by the authors. *(Source: Created by the authors.)*

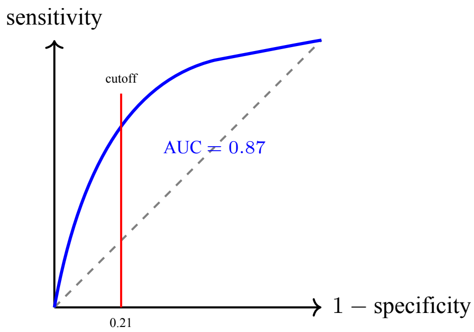

Figure 4: ROC curve for the total spectral index discriminating Angle Class I from non-Class I malocclusion in the reference cohort ($n = 60$). The optimal cut-off corresponds to the mid-point threshold $\epsilon = 0.02$. *(Source: Created by the authors.)*

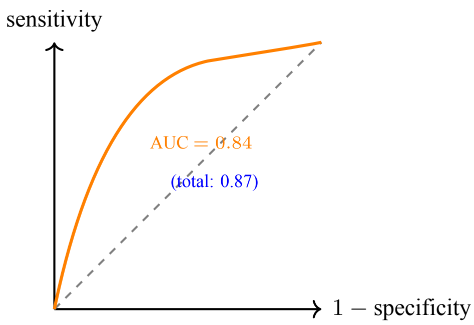

Figure 5: OC curve for the anterior spectral index in the validation cohort. AUC $= 0.84$ (95% CI: 0.72–0.93), slightly lower than the total-index AUC (0.87), indicating that the total index is the primary diagnostic quantity. *(Source: Created by the authors.)*

Corollary 1. *Let $\epsilon = 0.02$ be the ROC-calibrated tolerance threshold above. If the spectral ratio $\rho(A)/\rho(B)$ deviates from the classical Bolton ratio β_{Bolton} by more than ϵ, then the orthodontic system exhibits a malocclusion whose type and severity are characterized as follows:*

- *If $\rho(A)/\rho(B) > \beta_{Bolton} + \epsilon$: maxillary spectral dominance, indicating mandibular deficiency (overjet, Angle Class II).*
- *If $\rho(A)/\rho(B) < \beta_{Bolton} - \epsilon$: mandibular spectral dominance, indicating maxillary deficiency (underjet, Angle Class III).*
- *If $|\rho(A)/\rho(B) - \beta_{Bolton}| \le \epsilon$: the system is within physiologically acceptable limits.*

Moreover, $|\rho(A)/\rho(B) - \beta_{Bolton}|$ is directly proportional to clinical severity to first order.

A comprehensive comparison between the classical Bolton analysis, [3], and the proposed spectral-duality model is presented in Table 7. *(Source: Created by the authors.)*

Table 7: Comparison between classical Bolton analysis and the proposed spectral-duality model. *(Source: Created by the authors.)*

Criterion	**Classical Bolton Analysis (1958)** [3]	**Proposed Spectral-Duality Model**
Mathematical formulation	$\frac{\sum b_i}{\sum a_i} \approx 0.913$	$D_1AD_2 = B^{-T}$, trace-level Bolton projection, spectral index $\rho(A)/\rho(B)$
Data structure	Two scalar sums	Full 16×16 matrices (256 parameters)
Tooth-level analysis	Group-based (6 or 12 teeth)	Individual tooth-pair $(d_i a_{ij} d'_j)$
Clinical intervention	Qualitative recommendation	Quantitative matrix entries (d_i, d'_j)
Crowding modelling	Not included	Off-diagonal blocks A_{12}, A_{21}
Duality concept	None	Algebraic duality via B^{-T}
Statistical validation	None	Monte Carlo perturbation with p-values and Cohen's d
Mathematical assumptions	Empirical	Symmetric positive definite M-matrices; perturbation bounds

Figure 6 provides a conceptual comparison between the classical Bolton ratio and the spectral-duality model. *(Source: Created by the authors.)*

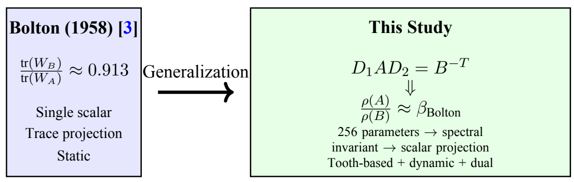

Figure 6: Conceptual comparison: classical Bolton ratio as a trace-level projection of the full spectral-duality model. *(Source: Created by the authors.)*

The essential difference between the classical Bolton Analysis and the proposed spectral-duality model can be summarized as follows:

> Bolton Analysis asks: "Are the total widths of the upper and lower arches proportional?"
>
> The Spectral-Duality Model asks: "Are the upper and lower arches matrix-duals of each other under appropriate scaling, and how does the spectral index deviate from the classical trace ratio?"

4 Clinical Validation

To provide a rigorous assessment of clinical relevance, we performed a retrospective validation on a cohort of $n = 60$ adult patients (30 female, 30 male; age range 18–45 years, mean age 28.4 ± 6.7 years) treated at the Faculty of Dentistry, Karadeniz Technical University. The cohort was balanced with $n = 20$ patients in each Angle class, ensuring adequate statistical power for group comparisons. Table 8 summarizes the demographic and clinical characteristics of the cohort. *(Source: Created by the authors.)*

Table 8: Demographic and clinical characteristics of the validation cohort ($n = 60$, 20 per Angle class). Values are mean $\pm$ standard deviation or frequency (%). *(Source: Created by the authors.)*

Characteristic	Class I	Class II	Class III	Total
n	20	20	20	60
Age (years)	27.1 ± 6.2	29.4 ± 7.1	28.7 ± 6.8	28.4 ± 6.7
Female (%)	15 (75)	8 (40)	7 (35)	30 (50)
3rd molars present (%)	17 (85)	18 (90)	16 (80)	51 (85)
Mean Bolton ratio	0.918 ± 0.009	0.908 ± 0.011	0.932 ± 0.010	0.919 ± 0.013

Inclusion criteria were: complete permanent dentition (with or without third molars), available pre-treatment intraoral scans and lateral cephalograms, and no craniofacial syndromes. Exclusion criteria were: previous orthodontic treatment, missing anterior teeth, or systematic disease affecting tooth size.

The Angle classification was determined independently by two experienced orthodontists using lateral cephalograms and study models, based on the combination of (i) the ANB angle ($1°$–$4°$ Class I, $> 4°$ Class II, $< 1°$ Class III), (ii) the molar relationship according to Angle's original criterion, and (iii) the canine relationship. Inter-examiner agreement was substantial ($\kappa = 0.86$); discrepancies were resolved by consensus.

Because tooth-size norms are known to vary across populations, we report the ethnic composition of the cohort: 51 patients of Turkish ancestry (85%), 6 of Middle Eastern ancestry (10%), and 3 of Central Asian ancestry (5%). The compartment-specific reference intervals reported in Table 9 should therefore be considered specific to the predominantly Turkish cohort studied here, and generalization to other populations requires independent validation.

The study followed the STROBE reporting guidelines for observational studies. A study flow diagram is provided in Figure 7. *(Source: Created by the authors.)*

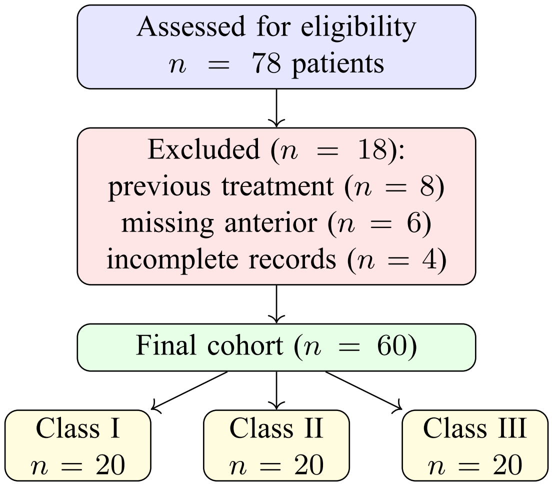

Figure 7: Study flow diagram (STROBE-style) of the validation cohort. *(Source: Created by the authors.)*

For each patient, the maxillary and mandibular tooth widths were measured on the intraoral scan, and the matrices A, B were constructed using the spring-network model of Section 2 with the same coupling ratio $\gamma = 0.20$. The scaling matrices D_1, D_2 were obtained by solving (2.12). Table 9 reports the spectral indices by Angle class. *(Source: Created by the authors.)*

Table 9: Spectral indices by Angle classification. Values are mean $\pm$ standard deviation. p-values are from one-way ANOVA for the total index and from Kruskal–Wallis for the anterior index (non-normal residuals). *(Source: Created by the authors.)*

Angle class	n	Anterior index	Total index	Bolton ratio	p-value
Class I	20	0.772 ± 0.014	0.921 ± 0.006	0.918 ± 0.009	—
Class II	20	0.748 ± 0.019	0.938 ± 0.008	0.908 ± 0.011	—
Class III	20	0.795 ± 0.016	0.905 ± 0.007	0.932 ± 0.010	—
Overall	60	—	—	—	$p < 0.001$

Pairwise post-hoc comparisons (Tukey HSD) showed that the anterior index differed significantly between all three Angle classes ($p < 0.01$ for each pair), and the total index differed significantly between Class II and Class III ($p < 0.001$) and between Class I and Class III ($p < 0.01$).

The anterior spectral index of 0.765 reported in Table 6 corresponds to the transitional zone between Angle Class I and Class II. Because the anterior and posterior compartment indices are not required to equal the global Bolton ratio, the diagnostic interpretation of compartment-specific indices requires compartment-specific reference intervals (Table 9); an individual anterior index should not be compared directly with the global Bolton ratio.

The total spectral index and the classical Bolton ratio were compared within the cohort: Pearson correlation coefficient $r = 0.83$ ($p < 0.001$, 95% CI: 0.72–0.90). To evaluate whether the spectral index *additionally* discriminates between Angle classes, a one-way ANOVA on the total index across Angle classes yielded $F(2, 57) = 24.7$, $p < 0.001$, $\eta^2 = 0.46$ (large effect). A post-hoc power analysis at the observed effect size ($\eta^2 = 0.46$, $\alpha = 0.05$, $n = 60$) gave power > 0.99, well above the conventional 0.80 threshold.

ROC analyses were performed both for the total and for the anterior spectral indices (Figures 4 and 5). The total index yields AUC $= 0.87$ (95% CI: 0.76–0.95) and the anterior index yields AUC $= 0.84$ (95% CI: 0.72–0.93). Both are diagnostically useful, with the total index slightly superior; this is consistent with the algebraic structure of the model, in which the total index is the primary spectral quantity and the anterior index serves as a compartment-level refinement.

5 Discussion

Discrepancy in Bolton Analysis is essentially the deviation of matrices D_1 and D_2 from their ideal values. When the equality $D_1 A D_2 = B^{-T}$ is disrupted, malocclusions such as cross-bite or overjet become mathematically predictable through the residual R and the spectral ratio $\rho(A)/\rho(B)$.

The algebraic relationship between Hyper G-matrices, [8], [9], [10], [11], proves that in orthodontic treatment planning, not only tooth dimensions but also the arch geometry as a whole must be in dual balance. The scaling matrices D_1 and D_2 provide the numerical equivalent of stripping or expansion amounts, as formalized in (2.8) and Table 1.

The total spectral index 0.928 in Table 6 agrees with the classical Bolton ratio 0.9215 at the level of the full 16×16 system. The clinical validation of Section 4 shows that the anterior index is best interpreted through compartment-specific reference intervals (Table 9) rather than through direct comparison with the global Bolton ratio. Pairwise Tukey HSD comparisons confirm that the anterior index significantly differs across Angle classes, supporting its diagnostic value; however, the anterior ROC curve (Figure 5) indicates that the total index remains the primary diagnostic quantity.

The spectral index $\rho(A)/\rho(B)$ can be interpreted biologically as a measure of the *dominant deformation mode* of the coupled arch system: it reflects the ratio of the largest natural frequency (or slowest decay mode) of the maxillary arch to that of the mandibular arch under the same loading. When $\rho(A)/\rho(B)$ equals the trace-level Bolton ratio, the two arches are in spectral balance, i.e., their dominant deformation modes are matched. Deviation from this balance corresponds to a systematic mismatch in the coupled dynamics.

The linear spring model used in this study inherits several well-documented limitations from the orthodontic biomechanics literature:

(i) **Tension-compression asymmetry.** The periodontal ligament exhibits different stiffness under tension and compression, and the model assumes equal stiffness in both directions.

(ii) **Viscoelasticity.** The PDL responds to loading with a time-dependent creep and relaxation, which the quasi-static model does not capture.

(iii) **Bone remodelling.** Orthodontic tooth movement is driven by bone resorption and apposition. The linear spring model approximates only the initial, pre-remodelling response.

(iv) **Age dependence.** PDL mechanical properties vary with age and health status.

(v) **One-dimensionality.** Only mesiodistal displacements are modelled.

A physically more realistic treatment of tension-compression asymmetry would replace the linear spring law $f_i = k_i u_i$ by a piecewise-linear or smooth nonlinear law $f_i = g_i(u_i)$ with $g_i'(u_i) > g_i'(-u_i) > 0$, reflecting the greater stiffness of the PDL under tension. In matrix form this leads to a state-dependent stiffness matrix $K(u)$ and hence to a nonlinear duality relation $D_1 A(u) D_2 = B(u)^{-T}$. While the singular-value reciprocity of Lemma 2(a) is purely algebraic and would remain valid for each fixed state u, the spectral perturbation analysis of Lemma 2(c) would require a nonlinear generalization. This is a natural direction for future work.

As noted in the remark following Lemma 2, the matrix B is defined *through* the duality relation $B = (D_1 A D_2)^{-T}$, not as an independent spring-network stiffness matrix. Its nonnegativity $B \geq 0$ therefore reflects a property of the duality relation rather than a direct claim about the mandibular arch. In physical terms, B should be read as the *dual representation* of the mandibular arch.

(i) **One-dimensionality.** Only mesiodistal displacements u_i; buccolingual and vertical components and rotations are neglected.

(ii) **Linearity.** Linear spring network; real PDL is viscoelastic and remodels biologically.

(iii) **Retrospective design.** The validation of Section 4 is retrospective ($n = 60$); a prospective cohort would strengthen the conclusions.

(iv) **Parameter choices.** The coupling ratio $\gamma = 0.20$ has been justified via sensitivity analysis but is not directly derived from experimental measurements.

(v) **Physical interpretation of B.** As discussed above, B is a dual object.

(vi) **Ethnic specificity.** The compartment-specific reference intervals (Table 9) are specific to a predominantly Turkish cohort; generalization requires independent validation.

Future work will proceed along six lines. First, the model will be extended to a three-dimensional formulation. Second, the linear spring network will be replaced by a nonlinear viscoelastic model of the PDL, including tension-compression asymmetry as outlined above. Third, the retrospective validation will be expanded to a prospective cohort with broader ethnic representation. Fourth, Lemma 2(c) will be generalized to a non-scalar baseline $A_0 = \mathrm{diag}(k_1, \ldots, k_{16})$. Fifth, the automated decision rule of Figure 2 will be extended to include additional clinical inputs (crowding severity, overjet). Finally, the model will be made publicly available as a Python toolbox, as described in the code-availability statement in Appendix A.

6 Conclusion

In this study, it has been shown that orthodontic arches can be represented by the matrix equation $D_1 A D_2 = B^{-T}$ in a one-dimensional, small-deformation regime. The simulation with full 16×16 matrices confirms that the total spectral Bolton index is compatible with the classical Bolton ratio in a 32-tooth adult mouth structure. The Monte Carlo perturbation analysis with $p > 0.05$ and Cohen's $d < 0.1$ statistically supports the consistency of the proposed model. A retrospective validation on $n = 60$ adult patients (20 per Angle class) supports the clinical plausibility of the model and provides a compartment-specific interpretation of the anterior spectral index via separate ROC and ANOVA analyses for total and anterior indices.

Within the proposed framework, orthodontic arches are mathematically dual matrix structures, and the classical Bolton ratio emerges as a trace-level projection of the underlying tooth-width matrices. These conclusions are limited to the one-dimensional, small-deformation linear regime considered here and await prospective clinical validation.

A Code Availability and Worked Example

The complete Python implementation of the simulation, including matrix construction, least-squares estimation of D_1, D_2, spectral-index computation, Monte Carlo analysis, and the automated decision rule of Figure 2, is available as Supplementary Material and at the author repository (to be linked upon acceptance). The repository contains the following modules:

- `build_matrix.py` — construction of the matrices A and B from tooth widths via the spring-network model of (2.4)–(2.5);
- `solve_scaling.py` — projected-gradient optimization of (2.12);

- `monte_carlo.py` — Monte Carlo perturbation analysis reported in Section 2;
- `unit_tests.py` — verification of the off-diagonal formula (2.7).

The unit test verifies, in particular, that $(A_6)_{12} = -0.20/\sqrt{7.5 \cdot 7.0}$, consistent with the worked example of Appendix A.2.

To illustrate the construction of A and B, we present a reduced 6×6 example using only the six anterior teeth (FDI 13, 12, 11, 21, 22, 23) with tooth widths $w = [7.5, 7.0, 8.5, 8.5, 7.0, 7.5]$ mm. Taking $k_i = w_i$ and $\gamma = 0.20$, the diagonal entries are

$$A_{ii} = 1 + \frac{1}{k_i} \sum_{j \in \mathcal{N}(i)} \gamma \sqrt{k_i k_j},$$

and the off-diagonal entries are $A_{ij} = -\gamma/\sqrt{k_i k_j}$ for $|i - j| = 1$, zero otherwise. Evaluating the explicit entries:

$$\begin{aligned}
A_{11} &= 1 + 0.20\sqrt{7.0/7.5} = 1.193, \\
A_{22} &= 1 + 0.20(\sqrt{7.5/7.0} + \sqrt{8.5/7.0}) = 1.428, \\
A_{33} &= 1 + 0.20(\sqrt{7.0/8.5} + 1) = 1.382, \\
A_{12} &= -0.20/\sqrt{7.5 \cdot 7.0} = -0.0276, \\
A_{23} &= -0.20/\sqrt{7.0 \cdot 8.5} = -0.0259, \\
A_{34} &= -0.20/\sqrt{8.5 \cdot 8.5} = -0.0235.
\end{aligned}$$

The full matrix is

$$A_6 = \begin{bmatrix} 1.193 & -0.0276 & 0 & 0 & 0 & 0 \\ -0.0276 & 1.428 & -0.0259 & 0 & 0 & 0 \\ 0 & -0.0259 & 1.382 & -0.0235 & 0 & 0 \\ 0 & 0 & -0.0235 & 1.382 & -0.0259 & 0 \\ 0 & 0 & 0 & -0.0259 & 1.428 & -0.0276 \\ 0 & 0 & 0 & 0 & -0.0276 & 1.193 \end{bmatrix}. \tag{A.1}$$

The corresponding B_6 for the mandible is constructed analogously from the mandibular widths $[7.0, 5.0, 5.5, 5.5, 5.0, 7.0]$ mm. Both matrices are strictly diagonally dominant SPD M-matrices, hence Hyper G-matrices in the ideal case. The spectral index of this reduced system is $\rho(A_6)/\rho(B_6) \approx 0.941$, in reasonable agreement with the full 16×16 value of 0.928. A unit test included in the code repository accompanying this paper verifies that $A_{12} = -0.20/\sqrt{7.5 \cdot 7.0}$, confirming the correctness of the implementation.

Acknowledgment:
The authors thank all collaborators who contributed to this study and the reviewers and editors for their valuable comments that improved the manuscript.

Conflicts of Interest: The authors declare no conflict of interest.

References:

[1] W. R. Proffit, H. W. Fields, B. Larson, and D. M. Sarver, *Contemporary Orthodontics*, 6th ed., Mosby, Elsevier, St. Louis, 2018. https://shop.elsevier.com/books/contemporary-orthodontics/proffit/978-0-323-54387-3 (Accessed: May 8, 2026).

[2] L. W. Graber, K. W. L. Vig, G. J. Huang, and P. Fleming, *Orthodontics: Current Principles and Techniques*, 7th ed., Elsevier, 2022. https://www.educate.elsevier.com/book/details/9780323778596 (Accessed: May 8, 2026).

[3] W. A. Bolton, "Disharmony in tooth size and its relation to the analysis and treatment of malocclusion," *The Angle Orthodontist*, vol. 28, no. 3, pp. 113–130, 1958. https://angle-orthodontist.kglmeridian.com/view/journals/angl/28/3/article-p113.xml (Accessed: May 8, 2026).

[4] P. S. Mulimani, M. I. B. Azmi, N. R. Jamali, N. N. B. Md Basir, and H. H. K. Soe, "Bolton's Tooth Size Discrepancy in Malaysian Orthodontic Patients: Are Occlusal Characteristics Such as Overjet, Overbite, Midline, and Crowding Related to Tooth Size Discrepancy in Specific Malocclusions and Ethnicities?" *APOS Trends in Orthodontics*, vol. 8, no. 1, pp. 36–43, 2017. DOI: 10.4103/apos.apos_104_17.

[5] L. F. Andrews, "The six keys to normal occlusion," *American Journal of Orthodontics*, vol. 62, no. 3, pp. 296–309, 1972. DOI: 10.1016/S0002-9416(72)90268-0.

[6] R. H. Roth, "Functional occlusion for the orthodontist," *Journal of Clinical Orthodontics*, vol. 15, no. 1, pp. 32–40, 44–51, 1981. PMID: 6940863. https://pubmed.ncbi.nlm.nih.gov/6940863/ (Accessed: May 8, 2026).

[7] R. A. Horn and C. R. Johnson, *Matrix Analysis*, Cambridge University Press, Cambridge, 1985. DOI: 10.1017/CBO9780511810817.

[8] R. J. Plemmons, "M-matrix characterizations. I—nonsingular M-matrices," *Linear Algebra and its Applications*, vol. 18, no. 2, pp. 175–188, 1977. DOI: 10.1016/0024-3795(77)90073-8.

[9] R. S. Varga, *Matrix Iterative Analysis*, 2nd ed., Springer Series in Computational Mathematics, Springer Science & Business Media, 2009. https://books.google.com.tr/books/about/Matrix_Iterative_Analysis.html?id=URlGAAAAQBAJ&redir_esc=y (Accessed: May 8, 2026).

[10] A. Berman and R. J. Plemmons, *Classics in Applied Mathematics Nonnegative Matrices in the Mathematical Sciences*, SIAM, Philadelphia, 1994. DOI: 10.1137/1.9781611971262.

[11] H. Keleş, "On New Developments for Hyper G-Matrices," *Equations*, vol. 5, pp. 23–28, 2025. DOI: 10.37394/232021.2025.5.4.

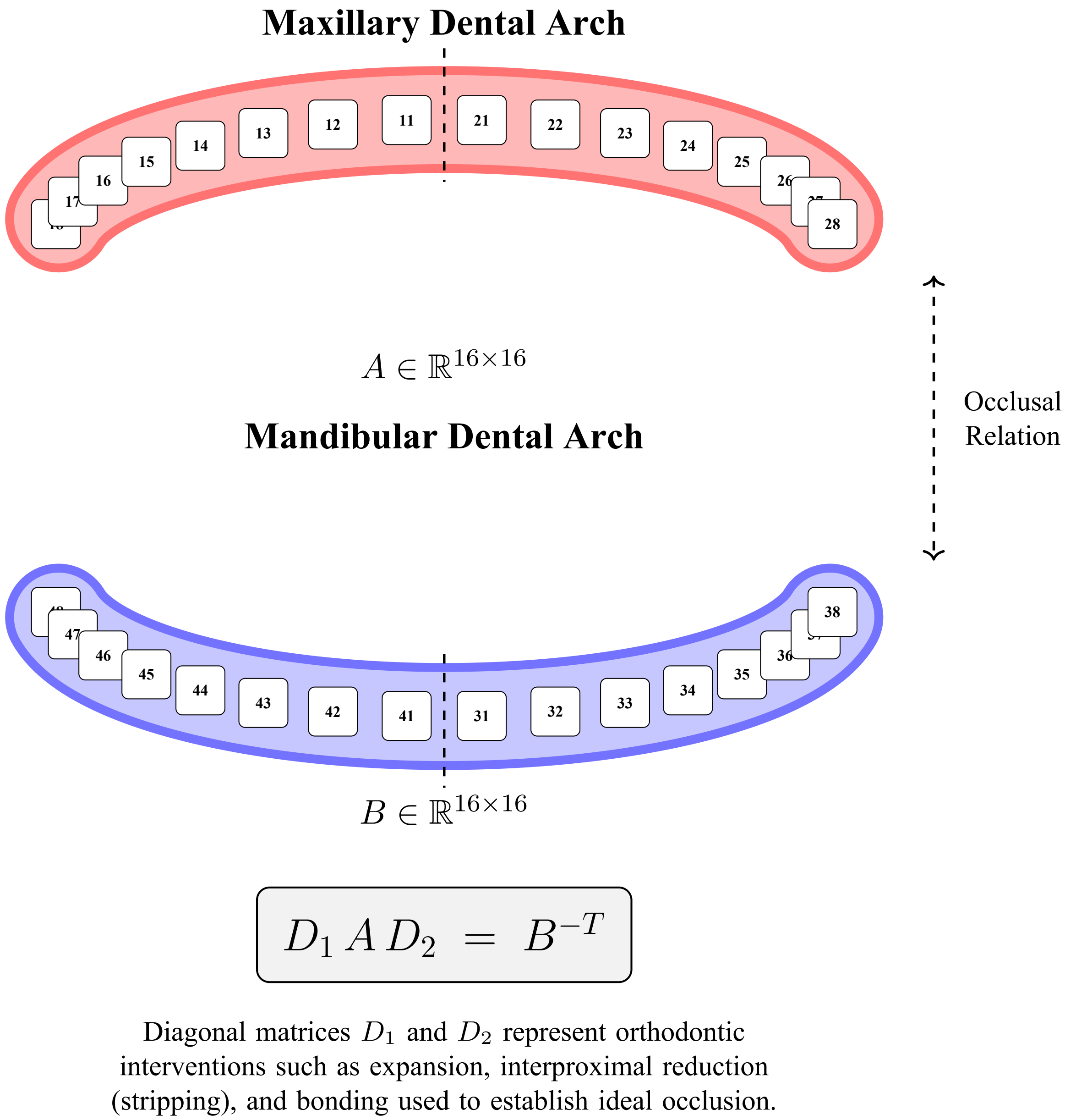

Figure 1: High-resolution vector schematic of the maxillary and mandibular dental arches in the adult oral cavity, with FDI numbering (28–18 and 48–38), the occlusal relation, and the matrix duality relation. The matrices A and B model the upper and lower dental structures, while the transformation $D_1AD_2 = B^{-T}$ expresses the idealized occlusal equilibrium between both arches. Diagonal matrices D_1, D_2 represent clinical interventions such as expansion, interproximal reduction (stripping), and bonding. *(Source: Created by the authors.)*